

# Effect of soil temperature on optical frequency transfer through unidirectional dense-wavelength-division-multiplexing fiber-optic links

T. J. Pinkert,<sup>1</sup> O. Böll,<sup>2</sup> L. Willmann,<sup>2</sup> G. S. M. Jansen,<sup>1</sup> E. A. Dijck,<sup>2</sup>  
B. G. H. M. Groeneveld,<sup>2</sup> R. Smets,<sup>3</sup> F. C. Bosveld,<sup>4</sup> W. Ubachs,<sup>1</sup>  
K. Jungmann,<sup>2</sup> K. S. E. Eikema,<sup>1</sup> and J. C. J. Koelemeij<sup>1,\*</sup>

<sup>1</sup>Department of Physics and Astronomy, LaserLaB, VU University, De Boelelaan 1081,  
1081 HV Amsterdam, The Netherlands

<sup>2</sup>Van Swinderen Institute for Particle Physics and Gravity, Faculty of Mathematics and Natural Sciences,  
Nijenborgh 4, 9747 AG Groningen, The Netherlands

<sup>3</sup>SURFnet, Radboudkwartier 273, 3511 CK Utrecht, The Netherlands

<sup>4</sup>KNMI, Utrechtseweg 297, 3731 GA De Bilt, The Netherlands

\*Corresponding author: j.c.j.koelemeij@vu.nl

Received 17 October 2014; revised 10 December 2014; accepted 11 December 2014;  
posted 12 December 2014 (Doc. ID 225128); published 23 January 2015

Results of optical frequency transfer over a carrier-grade dense-wavelength-division-multiplexing (DWDM) optical fiber network are presented. The relation between soil temperature changes on a buried optical fiber and frequency changes of an optical carrier through the fiber is modeled. Soil temperatures, measured at various depths by the Royal Netherlands Meteorology Institute (KNMI) are compared with observed frequency variations through this model. A comparison of a nine-day record of optical frequency measurements through the  $2 \times 298$  km fiber link with soil temperature data shows qualitative agreement. A soil temperature model is used to predict the link stability over longer periods (days–months–years). We show that optical frequency dissemination is sufficiently stable to distribute and compare, e.g., rubidium frequency standards over standard DWDM optical fiber networks using unidirectional fibers. © 2015 Optical Society of America

*OCIS codes:* (120.0120) Instrumentation, measurement, and metrology; (120.5050) Phase measurement; (120.6810) Thermal effects; (060.2300) Fiber measurements.

<http://dx.doi.org/10.1364/AO.54.000728>

## 1. Introduction

In recent years, fiber-optic connections in telecommunication networks have proven to be suitable for frequency comparisons and frequency distribution with high stability over long distances. In general, the frequency of either a continuous-wave (CW) laser or a microwave reference is transmitted over an

optical fiber and received at the remote site. Several experiments [1–7] have shown that frequency comparisons at or below the current accuracy level of the best atomic frequency references, a few times  $10^{-18}$  at  $>1000$  s [8–11], are feasible over long-haul fiber connections. For example, the optical frequency of the 1S–2S transition in atomic hydrogen was recently measured with respect to a remote Cs frequency standard with  $4.5 \times 10^{-15}$  relative uncertainty, employing a 920 km long fiber-optic link performing at the  $4 \times 10^{-19}$  at a 2000 s uncertainty level [6,12].

Fiber-optic methods for remote frequency comparison can provide significantly better stability than current satellite-based methods. These include two-way satellite time and frequency transfer (TWSTFT) [13–15] and (carrier-phase) common-view global positioning system [(CP)/CV-GPS] comparisons [16–18]. The accuracy limits of satellite-based methods are of the order of  $10^{-15}$  at one day [18–20], which is already insufficient to compare state-of-the-art cesium fountain clocks operating at less than  $5 \times 10^{-16}$  at  $\geq 3 \times 10^4$  s uncertainty level [21,22].

Plans for high-resolution laser spectroscopy experiments at VU University Amsterdam LaserLaB and at Van Swinderen Institute, University of Groningen, would be greatly facilitated by direct frequency comparisons over an optical fiber link at stability levels better than  $10^{-14}$  at  $< 1000$  s. For this purpose, a  $2 \times 298$  km fiber-optic connection between both laboratories has been established using a  $2 \times 295$  km dense-wavelength-division-multiplexing (DWDM) channel provided by SURFnet. The top part of Fig. 1 gives an overview of the SURFnet fiber network in the Netherlands. The optical path between VU University Amsterdam and Van Swinderen Institute Groningen is marked in green. The bottom part shows the details of the optical path.

The link consists of two unidirectional fibers. Interferometric detection and active compensation of fiber length changes [23] is therefore not possible. However, it is possible to create a bidirectional path in the optical fiber, and implement a compensation system [7]. It must be noted that, in contrast to some of the other frequency comparison links [1,2,4–6], our link is part of a carrier-grade DWDM optical network in which the fiber is shared with other users, and several other wavelength channels are simultaneously used for data transfer.

The use of a standard DWDM channel enables us to characterize the performance of unidirectional transmission of optical frequency references in public transport networks carrying live network traffic. Here the performance is characterized in terms of frequency instability (Allan deviation). For long underground fiber links, the frequency instability has been attributed primarily to length changes induced by soil temperature variations. The main aim of this work is to provide quantitative insight into this phenomenon by modeling the soil-temperature-induced length variations and the resulting frequency instability of the fiber link, and by comparing measured frequency instabilities with predictions by the model.

Unidirectional frequency transfer will be useful for institutions and industries that require accurate and reliable time and frequency references. Optical frequency distribution may be used for calibration purposes, such as accurate length, and, in the future, mass measurements (through the Josephson effect and the Watt balance) by referencing to the SI second.

This article is structured as follows: in Section 2, a model for the influence of temperature on the

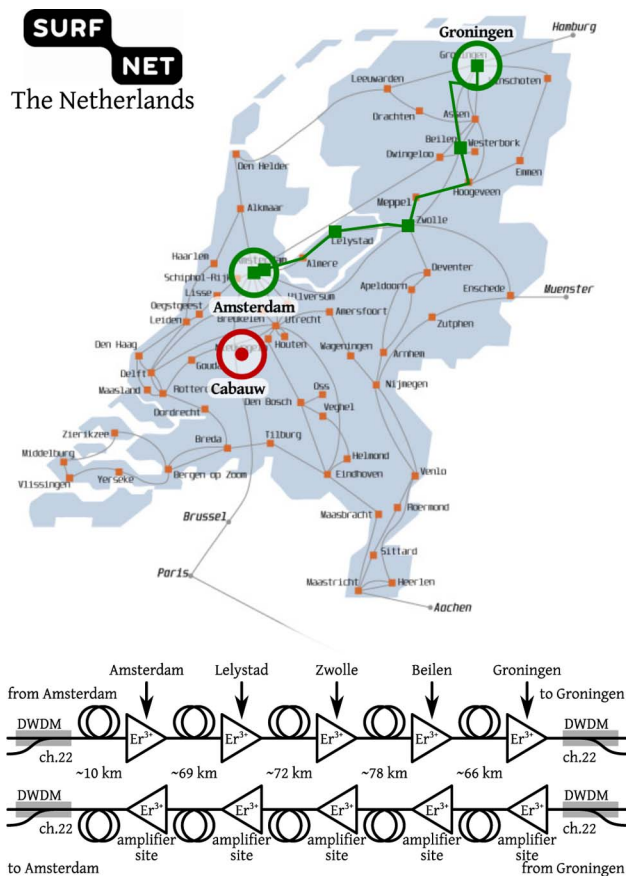


Fig. 1. Top: schematic map of the SURFnet fiber-optic network. The fiber link between VU University Amsterdam and Van Swinderen Institute Groningen is shown by the green line. The green squares are amplifier sites. the red circle is the KNMI measurement site at Cabauw. Bottom: schematic representation of the duplex fiber link between Amsterdam and Groningen in the SURFnet network (length:  $2 \times 295$  km). The unidirectional  $\text{Er}^{3+}$  amplifiers are used by all active DWDM channels. In Amsterdam,  $\sim 500$  m of intra-office fiber bridges the distance between the SURFnet node and the laboratory. In Groningen,  $\sim 2$  km of additional underground fiber is needed to bridge the distance from the SURFnet node at the computing center of the University of Groningen to the laboratory, adding to a total link length of  $2 \times 298$  km.

stability of fiber-optic frequency transfer is presented, along with a soil temperature model. In Section 3, we present our approach to determine the stability of the  $2 \times 298$  km optical frequency link, including details of the setups used in Amsterdam and Groningen, as well as technical details specific to the use of nonstandard equipment in fiber networks carrying live data of other users. Results are discussed in Section 4, followed by conclusions and an outlook presented in Section 5.

## 2. Theory: Frequency Stability of the Fiber Link and Soil Temperature

The phase  $\phi$  accumulated by a monochromatic light wave guided along a certain path of length  $L$  and effective refractive index  $n$  can be written as

$$\varphi = \frac{\omega_0}{c} nL, \quad (1)$$

where  $\omega_0$  is the frequency of the light (in radians per second). Several physical processes can lead to phase (and thus frequency) variations in fiber-optic links.

At short time scales (<100 s), environmental vibrations couple to the fiber and can therefore cause path length variations, e.g., via stress-induced refractive index variation, which may occur at frequencies up to tens of kilohertz. At time scales longer than 1 s, significant phase variations also occur because of thermal expansion of the fiber and thermally induced changes in the refractive index. These variations are typically slow, and, for a fiber that is installed mainly underground in an outdoor environment, they are mostly affected by the diurnal and seasonal soil temperature cycles [24]. Our work is focused on the understanding of the long-term stability of fiber links in relation to such temperature variations.

The phase variations due to a time-varying temperature  $T$  are

$$\frac{d\varphi}{dt} = \frac{\omega_0}{c} \left( L \frac{\partial n}{\partial T} \frac{dT}{dt} + n \frac{\partial L}{\partial T} \frac{dT}{dt} \right). \quad (2)$$

We can express the relative length variations of the fiber as a function of temperature as

$$\frac{1}{L} \frac{\partial L}{\partial T} = \alpha_\Lambda, \quad (3)$$

where  $\alpha_\Lambda$  is the thermal expansion coefficient of the fiber. Furthermore, it is customary to write

$$\frac{\partial n}{\partial T} = \alpha_n, \quad (4)$$

with  $\alpha_n$  the thermo-optic coefficient. Note that both  $\alpha_\Lambda$  and  $\alpha_n$  are weakly dependent on temperature, which we ignore here.

A typical (room-temperature) value of the thermal expansion coefficient of the fiber glass is  $\alpha_\Lambda = 5.6 \times 10^{-7}/^\circ\text{C}$  [25]. The thermo-optic coefficient has a typical value of  $\alpha_n = 1.06 \times 10^{-5}/^\circ\text{C}$  [25], and is, therefore, the main cause of phase variations due to temperature changes. Similar effects due to varying air pressure are approximately 2 orders of magnitude smaller [26] and have, therefore, not been included in the model.

Considering the heat flux in isotropic media (soil) for a vertical temperature gradient and varying temperature, and modeling the temperature variation as a sinusoidal periodic signal, Van der Hoeven and Lablans [27] derive the equation for the temperature of the soil at a certain depth  $z$  and time  $t$  as

$$T(z, t) = T_0 + A_{T_0} e^{-zC_\varphi} \times \sin\left(\frac{2\pi}{P_{T_0}}(t - t_0) - zC_\varphi\right), \quad (5)$$

where  $T_0$  is the average temperature at the surface ( $z = 0$ ),  $A_{T_0}$  is the amplitude of the temperature

variation at the surface with period  $P_{T_0}$ , and  $t_0$  is an arbitrary time offset. The phase constant

$$C_\varphi = \frac{1}{C_s} \sqrt{\frac{\pi}{P_{T_0}}} \quad (6)$$

includes the soil constant  $C_s$ , which is determined by the thermal conductivity  $\lambda$ , the specific heat capacity  $C_m$ , and the mass density  $\rho$  of the soil according to

$$C_s = \sqrt{\lambda/\rho C_m}. \quad (7)$$

Equation (5) can be applied to both diurnal and annual variations in temperature. A remark must be made that accurate modeling of the soil temperature is delicate and involves, among other elements, the groundwater levels and groundwater freezing rates in winter [27].

In this model the amplitude of the temperature wave decreases exponentially with depth, while it undergoes a phase shift linear with depth. The equation is universal and can also be applied to other materials as long as the physical properties  $\lambda$ ,  $\rho$ , and  $C_m$  are known.

With the help of Eq. (5), average frequency deviations  $\Delta f$  from the nominal frequency  $f_0 = \omega_0/2\pi$  can be calculated for any depth, using Eq. (2) for temperature differences  $\Delta T$  over a time interval  $\Delta t$  as

$$\Delta f = 2\pi f_0 \frac{L}{c} (\alpha_n + n\alpha_\Lambda) \frac{\Delta T}{\Delta t}. \quad (8)$$

### 3. Experimental Methods

To characterize the frequency stability of the fiber link, two different methods are used. The first method consists of the one-way transmission of a C-band-wavelength CW laser, locked to a mode of an Er<sup>3+</sup>-doped fiber frequency comb laser in Amsterdam. In Groningen, the transmitted laser frequency is measured using a similar frequency comb laser. Both frequency combs are locked to GPS-disciplined atomic clocks. Therefore, the stability of the optical frequency measurements in Amsterdam and in Groningen depends on the fiber link as well as the atomic clock stabilities. The second method employs a closed fiber loop Amsterdam–Groningen–Amsterdam. In this case the laser frequency can be compared with itself after its round trip through the fiber loop. The second method takes advantage of the fact that the laser frequency instability on the time scale of the measurement is much smaller than the instabilities introduced in the fiber loop.

Figure 2 gives an overview of the measurement setup that is used to characterize the frequency stability of the fiber link. A narrow-linewidth CW laser [Redfern Integrated Optics Inc. (RIO) Planex, 3 kHz Lorentzian linewidth, 20 mW output power, and wavelength 1559.79 nm (International Telecommunication Union, ITU channel 22)] is phase locked to the fiber frequency comb laser (Menlo Systems

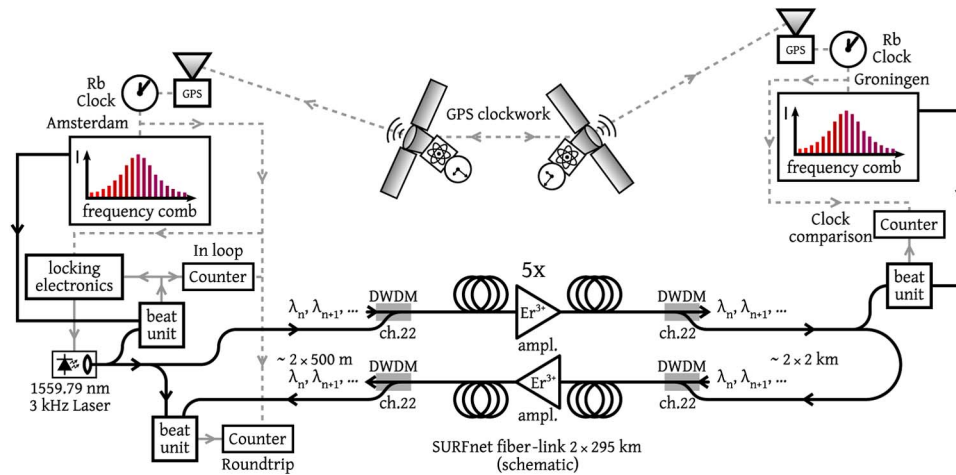


Fig. 2. Amsterdam–Groningen fiber link, overview of the experimental setup. This arrangement allows for optical-versus-GPS comparisons (essentially a fiber-optic frequency comparison of the GPS-linked Rb clocks in Amsterdam and Groningen), and for measurements of the round-trip stability of the fiber-link in Amsterdam. Details of the CW laser lock setup are given in Fig. 3. The setup for the round-trip analysis and for the optical versus Rb/GPS comparison are shown in detail in Fig. 4 and Fig. 5, respectively.

FC1500) and used as an absolute optical frequency reference. To verify the lock quality, the in-loop beat signal is counted. The optical reference frequency is sent to Groningen via the fiber link. The nominal length  $L$  of the fiber link is  $2 \times 298$  km between the laboratories in Amsterdam and Groningen. The optical fibers of the pair are located in a fiber-bundle and thus follow nearly the same physical path.

In the SURFnet DWDM system, other wavelength channels transport 10 Gbps (non-return-to-zero amplitude modulation) and 100 Gbps (polarization-multiplexed quadrature phase-shift keying) data. Nonlinear cross talk between these channels and the channel used for frequency transfer is avoided by limiting the average launch power to 0 dBm per span per wavelength, and to  $-4$  dBm per wavelength when launched into a dispersion compensation module. Intrachannel cross talk is avoided by reserving (ITU) channel 22 exclusively for the link Amsterdam–Groningen, i.e., this channel is not used in other segments of the DWDM system. We incorporated several measures to stabilize the power of the CW laser launched into the DWDM link. First, the launch power is actively stabilized to  $(0 \pm 0.5)$  dBm using a variable optical attenuator controlled by a feedback loop. Second, temperature stabilization is needed, as this prevents thermally induced mode hops to wavelengths that fall outside ITU channel 22, and that are converted to power jumps by the DWDM filters in the system. Apart from the phase lock to the frequency comb mentioned above, the temperature of the CW laser is stabilized by a two-stage temperature controller to within 10 mK. Mode hops are furthermore avoided by proper rf decoupling of the laser current control electronics from their electrical environment.

In Groningen the light is split. Part of the light is used in a frequency comparison against the local optical frequency standard (Menlo Systems FC1500), while the other part of the light is sent back to

Amsterdam (received power 0–6 dBm). As pointed out above, the comparison of the frequency of the light after the round trip with the CW laser source reveals the noise contribution from the fiber link.

Both optical frequency combs are locked to rubidium (Rb) frequency standards (SRS FS725), which are disciplined to the 1 pulse per second output of GPS receivers (Amsterdam: Trimble Acutime 2000, Groningen: Navsync CW46). The combined instability of the GPS-receiver output and Rb clocks is transferred to the frequency comb lasers via the various rf locks used to stabilize the frequency comb laser repetition rate frequency  $f_{\text{rep}}$  and carrier envelope offset frequency  $f_{\text{CEO}}$ .

Figure 3 shows the details of the CW laser stabilization setup. Part of the light of the diode is split off and fed to a fiber-based beat-note unit consisting of a DWDM filter to reject a large part of the frequency comb spectrum, a fused coupler, and a fiber-coupled photodiode ( $\sim 2$  GHz bandwidth,  $50/125$   $\mu\text{m}$  multi-mode fiber coupled) to detect the rf beat signal. The rf beat signal ( $f_{\text{beat}} = 60$  MHz) is bandpass filtered (filter bandwidth  $> 10$  MHz) and amplified before comparison with a signal generator (Agilent 33250A, referenced to the Rb clock), via counting phase detector electronics. Feedback on the diode laser phase is achieved via a fast PID controller acting directly onto the diode-laser injection current (bandwidth  $> 1$  MHz).

To verify proper CW-laser locking conditions during the experiment, the in-loop rf beat frequency is recorded with a Rb-referenced counter. For dead-time-free counting of rf frequencies, either a quasi-continuous double Agilent 53132A counter setup is used, or an Agilent 53230A counter in a continuous reciprocal frequency counting mode.

To characterize the stability of the fiber link, the setup of Fig. 4 is used. Light of the diode laser is split by a fused coupler. Part of the light is sent via the round-trip Amsterdam–Groningen–Amsterdam,

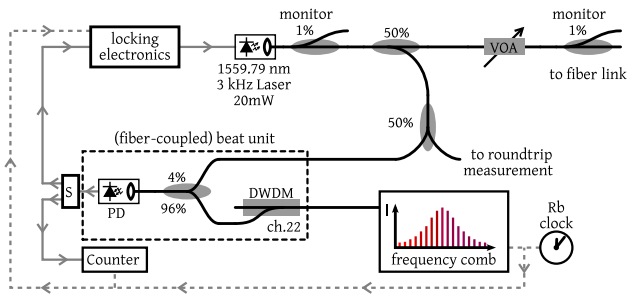


Fig. 3. CW-laser stabilization setup (Amsterdam). The 1559.79 nm, 3 kHz (Lorentzian linewidth) diode laser is frequency stabilized by a phase-locked loop to a mode of the  $\text{Er}^{3+}$ -fiber frequency comb laser. The photodiode signal of the fiber-coupled beat unit is amplified, filtered, and split by a 3 dB power splitter (S) for input to the phase detector and the counter. The stabilization setup is fully referenced to the GPS-disciplined Rb frequency standard. The monitor ports are used to observe optical power variations of the Planex laser before and after the variable optical attenuator (VOA), which regulates the laser power to a constant level before injection into the telecommunication network.

while another portion of the light is frequency shifted by an acousto-optic modulator (AOM). The output of the AOM is combined with the round-trip optical signal after transmission by the fiber link (power  $\sim -3$  dBm) and the beat frequency is detected with a fiber-coupled photodiode. Apart from wideband ( $>10$  MHz) rf filters, the beat-note signal was not filtered. Any frequency variations introduced by the fiber link can be measured as frequency deviations from the AOM frequency, which is generated by a Rb-referenced direct digital synthesizer (DDS) (Analog Devices AD9912).

To measure the round-trip stability, two different AOM and counter setups were used during the experiments. Initially an Agilent 53230A counter in reciprocal continuous mode was used to count the beat frequency of a free-space double-pass AOM unit (300 MHz) to obtain the results of Section 4.B. The free-space AOM has a polarization-dependent efficiency, which converts polarization changes due to slowly changing fiber birefringence to unwanted power variations in the AOM output beam. To over-

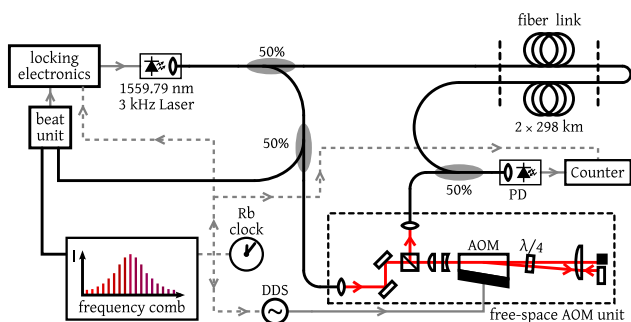


Fig. 4. Experimental setup for the characterization of the passive frequency stability of the fiber link (Amsterdam). For the long round-trip measurements, the free-space AOM unit (300 MHz) was replaced by a fiber-coupled AOM ( $-42$  MHz). In both cases the AOM was driven by a Rb-referenced DDS unit with a set accuracy of  $\sim 3.55$   $\mu\text{Hz}$ . Frequency deviations of the link are recorded with a Rb-referenced counter.

come this, the free-space AOM was later replaced by a polarization-insensitive fiber-coupled AOM (frequency shift  $-42$  MHz). The lower frequency of this AOM allowed using a channel of a high-end zero-dead-time K+K FMX-50 counter to count the beat frequency (used to obtain the results of Section 4.A).

The remote (Groningen) optical frequency characterization setup is depicted in Fig. 5. The link laser is amplified using a semiconductor optical amplifier, and guided to a free-space beat unit. The beat frequency is counted using a K+K FMX-50 counter. The frequency comb laser and counters are frequency referenced to the Rb standard.

#### 4. Measurements and Simulations

Two series of measurements have been performed on the fiber link, namely, an “optical-versus-GPS” measurement, for which the optical frequency is measured simultaneously at Amsterdam and Groningen and compared, and a round-trip measurement at the Amsterdam site (Fig. 2). It is known that soil temperature variations of the fiber may lead to significant frequency instability (see, for example, [28]). In this section, we present a model to describe and predict the influence of soil temperature variations on the frequency stability of underground fiber links. The results of the temperature model are compared with actual soil temperature and link stability measurements.

Apart from the instability contributed by the fiber link, the stability of the frequency transfer is limited by three sources. First, the stability of the frequency comb laser is limited by the Rb/GPS rf reference oscillator used to control the parameters of the comb. This reference has a specified relative instability of  $<10^{-11}$  at 1 s and below  $10^{-12}$  between  $10^3$  and  $10^5$  seconds, with a minimum around  $3 \times 10^{-13}$ . This long-term frequency instability is transferred to the CW link laser through the various rf locks in the setup.

The rf locks themselves also contribute to the frequency instability, which we assess as follows. Using a second, similar, CW laser (RIO Orion) locked

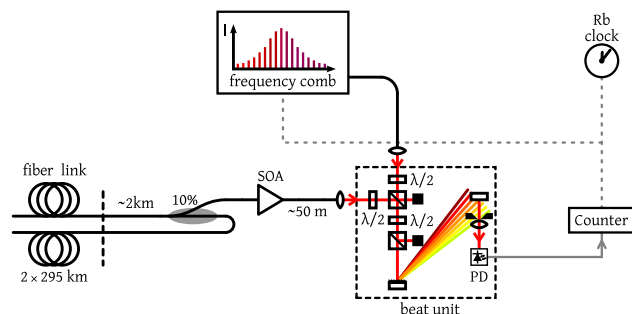


Fig. 5. Experimental setup for the remote optical frequency measurement (Groningen). Of the received optical power, 90% is sent back to Amsterdam. To improve the signal of the free-space beat unit, the link light is amplified with a BOA-6434 semiconductor optical amplifier (SOA). The amplified light is then combined with light from the fiber frequency comb laser in a free-space beat unit to obtain an rf beat between the nearest frequency comb mode and the CW link laser.

to the frequency comb, and employing the virtual beat note technique [29], the combined instability of the locking electronics is determined to be  $<9.1 \times 10^{-16}$  at 1 s. Thus, on time scales longer than 1 s, the rf noise is effectively averaged out so that its influence on the link measurements may be neglected.

A second source of instability plays a role in the round-trip measurements, for which a frequency drift of the laser source may lead to an apparent frequency shift of the (delayed) light transmitted by the fiber loop. Considering the 3.2 ms round-trip propagation delay of the light over the fiber link, the (linear) drift of the frequency standard ( $10^{-11}$  at 1 s) plays a role only at the level of  $3.2 \times 10^{-14}$  at 1 s, decreasing as  $\sim 1/\tau_{\text{gate}}$ , the inverse of the counter gate time, due to the fractional time overlap  $(\tau_{\text{gate}} - \tau_{\text{roundtrip}})/\tau_{\text{gate}}$  between reference and round-trip light in the frequency comparison. This is 1 order of magnitude smaller than the typically measured link stability at 1 s, and averages down more rapidly with increasing  $\tau$ .

For the optical-versus-GPS comparison, a third source of instability is due to the fact that the Rb clocks in Amsterdam and Groningen are independently locked to GPS time. Small intrinsic phase differences between GPS signals, received at geographically separated locations, thus propagate through the frequency locks, and may manifest as additional noise in the link frequency measurement.

#### A. Fractional Frequency Transfer Stability over a $2 \times 298$ km Optical Fiber Link

The intrinsic frequency transfer stability of a fiber link is best measured on a closed loop, so that the frequency of the input signal can be directly compared with that of the round-trip signal. Figure 6 shows the results of two round-trip stability measurements. The first measurement is based on a 13 h time series of frequency measurements acquired on 6 July 2012, using the free-space AOM unit (Fig. 4) while recording with the Agilent 53230A. For this dataset, the absolute frequency of the round-trip optical signal was calculated and used to determine the overlapping Allan deviation (ODEV).

To compare the measurement with the soil temperature model, statistics on the scale of several days are needed. Therefore, a longer round-trip stability measurement took place from 30 September 2013 to 9 October 2013, using the fiber-coupled AOM while recording with the K+K FMX50 counter. This measurement contains a few periods during which the beat signal was too low for the FMX50 input circuits to record properly, leading to frequency outliers. Outliers were removed according to Chauvenets criterion [ $P = 0.5$ , 4102 datapoints (0.52% of the total set) removed] and were replaced with the median of the dataset. We have verified that the ODEV statistics are not influenced significantly by this operation.

#### B. Clock Transfer Stability

In the previous section we established that, for averaging periods of more than 10 s, the frequency

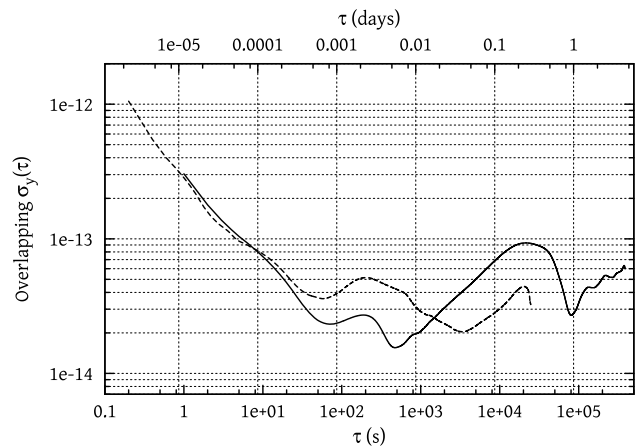


Fig. 6. Comparison of two round-trip stability measurements (ODEV, here denoted as Overlapping  $\sigma_y$ ) for averaging time  $\tau$ . Measurement of almost nine days from 30 September 2013 to 9 October 2013 (solid, outliers due to accidental low beat signal in this period where taken out and replaced with the median of the dataset, see text). The peak at 0.5 days and dip at 1 day are typical for frequency deviations with a one-day period. Measurement of more than 13 h performed on 6 July 2012, all data were included (dashed).

transfer instability of the link is  $<1 \times 10^{-13}$ . Given the stability of the laboratory frequency standards (Rb clocks) it is therefore to be expected that a direct measurement of the link laser frequency at the remote site (Groningen) yields the mutual clock stability. During the 2012 measurement session, the absolute laser frequency at the remote site was recorded. The result of this measurement, the round-trip stability, and the stability of the link laser lock frequency are presented in Fig. 7.

The link laser frequency was determined with respect to the frequency comb, taking into account variations of  $f_{\text{rep}}$  and  $f_{\text{CEO}}$ . The determination of the absolute laser frequency is limited by the resolution of the  $f_{\text{rep}}$  counter to  $2.5 \times 10^{-13}/\text{s}$ . The maximum observable round-trip instability is therefore about  $1 \times 10^{-15}/\text{s}$ . The observed instability is significantly higher, showing that the fiber may already influence the round-trip stability at the second time scale.

The frequency of the laser used for the characterization of the remote link was determined with respect to the nearest frequency comb mode. Together with the mode number determination, this directly delivers the remote absolute optical frequency. As can be seen in Fig. 7, the link laser frequency instability at the remote site is much larger than the total round-trip instability. Therefore, the local frequency references are the limiting factor. This means that we have effectively performed a frequency comparison between the GPS referenced Rb atomic clocks over the fiber link. Under the assumption of equal but independent clocks and frequency noise, the frequency instability is divided by  $\sqrt{2}$  to yield the stability of each individual setup and, thus, to enable the comparison with the

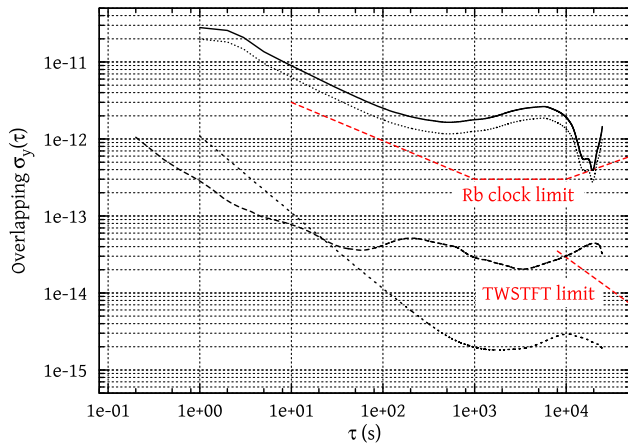


Fig. 7. Comparison of ODEVs of the in-loop link laser stability relative to the frequency comb (short dashed), the round-trip stability (long dashed), and the remote link laser frequency stability measured in Groningen (solid) of the 13 h 2012 measurement series, divided by  $\sqrt{2}$ , giving the Rb clock stabilities (dotted). The (red) straight dashed lines schematically indicate the Rb clock limit (SRS PRS10 datasheet), and the TWSTFT limit reported in [14].

instability of the Rb clock (Fig. 7). The measured performance is slightly worse than expected based on the Allan variance graph in the datasheet ( $<10^{-12}$  at  $>100$  s) of the clocks. This is possibly due to imperfect GPS reception, and/or uncorrelated frequency noise in the RF locks of the fiber combs to the Rb atomic clocks.

### C. Limits on Frequency Transfer Stability due to Soil Temperature Fluctuations

Based on coarse estimates we expected (soil) temperature fluctuations to have a major influence on the passive stability of the fiber link. The Royal Netherlands Meteorological Institute (KNMI) provided us with soil temperature measurements taken at the Cabauw site (see Fig. 1). Temperatures are measured at depths of 0, 2, 4, 6, 8, 12, 20, 30, and 50 cm every 12 s and averaged over 10 min intervals. Out of five KNMI locations, the site at Cabauw is the only location for which soil temperature data with such high temporal resolution is available in the Netherlands. The provided datasets consist of one set covering the nine-day link measurement with a 12 s time interval in October 2013 [30], and a 2-year dataset (2011, 2012) with a 10 min interval [31].

Equation (8) is used to convert these temperature series to frequency deviations expected on a  $2 \times 298$  km fiber link with the given thermal expansion and thermo-optic coefficients. In the next sections we use these reference data to compare the link stability with the soil temperature model given by Eq. (5).

### 1. Soil Temperature and Frequency Transfer Stability

The raw frequency data from the nine-day link stability measurement is compared to the frequency deviations as derived from the KNMI soil temperature

dataset over the same time period. The first question that needs to be addressed is to what extent such a comparison, correlating temperature effects measured in locations separated by tens of kilometers, is meaningful. The Cabauw measurement site (Fig. 1) is located more than 40 km south of the (geographically) 200 km long trajectory of the fiber. Therefore, the exact trends in soil temperature at the Cabauw site and along the fiber link can differ, due to local variations in solar irradiation and precipitation. Nevertheless, significant temperature correlations are expected as the different locations are relatively close, as seen from a meteorological and climatological point of view.

Figure 8 shows the round-trip stability in comparison to the fiber-link stability calculated from the KNMI soil temperature data. KNMI aims at a relative accuracy among sensors of 0.01 K and an absolute accuracy of 0.1 K. The noise in the soil temperature measurements amounts to a few mK. More accurate soil temperature observations will be difficult to make, let alone capturing all relevant variations along the optical path. All stabilities derived from soil temperature show a  $1/\tau$  slope for shorter time scales, which indicates the presence of white noise in the temperature measurements that does not appear in the fiber link instability. The noise levels at these time scales obscure frequency drift due to the daily temperature cycle. This cycle leads to the rising slope at longer time scales, with a local maximum at an averaging time of half a day. On even longer time scales, this instability cycle continues with a one-day period, and with local maxima decreasing in height over time. This is most clearly seen in the surface temperature curve.

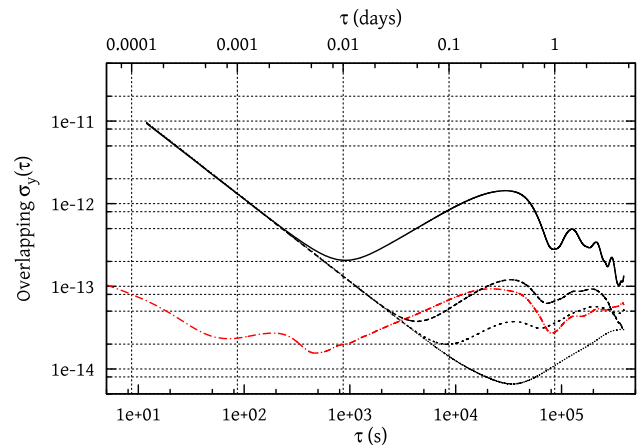


Fig. 8. Fiber-link round-trip stability (dashed-dotted) compared with round-trip stabilities as calculated from the KNMI soil temperature measurements for different fiber depths: on the surface (solid curve), at 20 cm depth (long-dashed curve), at 30 cm depth (short-dashed curve), and at 50 cm depth (dotted curve). At shorter averaging times, the model curves display a  $1/\tau$  slope, which indicates that, on shorter time scales, temperature noise is significantly more prominent in the KNMI measurements than in the temperature-dependent link stability.

The measured round-trip stability curve shows averaging at short time scales of less than 100 s, while at time scales larger than 1000 s, frequency drifts due to the diurnal temperature cycle dominate the instability. For averaging times longer than  $4 \times 10^3$  s, the link measurement shows qualitative agreement with the KNMI data at depths of 20–30 cm. The origin of the level of instability at time scales less than  $4 \times 10^3$  s remains unclear. Possible causes are the several hundreds of meters of the fiber link located inside buildings, which are subject to significant and relatively fast temperature variations (due to, e.g., airconditioning systems), while other factors like stress-induced frequency fluctuations cannot be entirely ruled out. We also considered the effect of polarization mode dispersion, which we find to be negligible. For a worst-case differential group delay of  $0.2 \text{ ps}/\sqrt{\text{km}}$ , the maximum polarization-dependent differential delay is  $\pm 5 \text{ ps}$  in our link. We typically observe polarization changes of  $10^\circ$  per hour, leading to fractional frequency deviations smaller than  $1.5 \times 10^{-16}$ . This is negligible compared to the observed frequency instability.

The correlation between soil temperature and link frequency drift can be inferred from the temperature and frequency measurement time series. To this end, the round-trip frequency deviations from the AOM frequency,  $\Delta f$ , are compared to the frequency deviations  $\Delta f_n$  due to soil temperature  $T_{\text{KNMI},n}$  at depth  $n$ , estimated using Eq. (8). Both datasets are averaged over 2 h windows to reduce noise levels. Figure 9 shows the raw data of the nine-day link measurement in comparison with  $\Delta f_n$  at 20 and 30 cm depth (2 h averages).

The depth at which the fiber link is buried is not precisely known, and it furthermore may vary along the path of the link. An estimate of the “effective” depth of the link may be obtained by assigning a weighting factor  $c_n \geq 0$  to each time series  $\Delta f_n$ , and minimizing (by least squares fitting) the difference  $y$  between the measured and calculated frequency deviations:

$$y = \Delta f - \sum_{n=0}^N c_n \Delta f_n(T_{\text{KNMI},n}) + f_{\text{offset}}. \quad (9)$$

The frequency offset parameter  $f_{\text{offset}}$  is needed to include a systematic offset between the link measurement data and the KNMI data. Such an offset may be caused by an overall relative temperature change between the fiber link path and the Cabauw site.

Figure 10 shows the variation of the fit parameters  $c_n$  and  $f_{\text{offset}}$  over time. These parameters and their time dependence are obtained as follows. First, all input data (i.e., the measured frequency deviations and the frequency deviations estimated from soil temperature measurements) are averaged with a 1 h window. Of the averaged datasets, a 24 h subset is taken (labeled by the median of the time stamps in

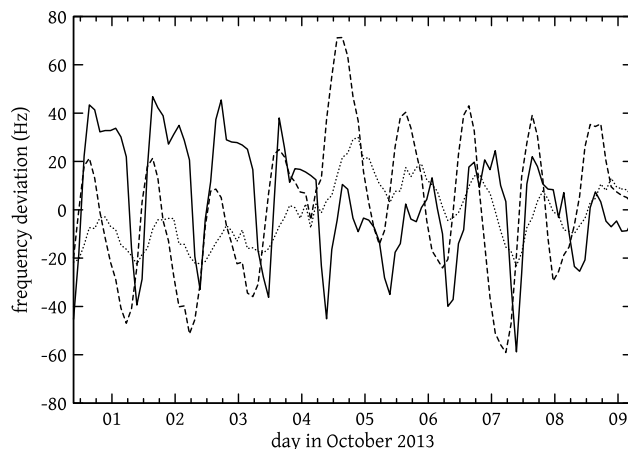


Fig. 9. Frequency deviations after a roundtrip through the fiber link (solid) and frequency deviations calculated from the soil temperature data at 20 cm (dashed) and 30 cm depth (dotted).

the set), for which the coefficients  $c_n$  and  $f_{\text{offset}}$  are found by least-squares fitting. This last step is repeated for a 24-h subset, which is offset by 6 h with respect to the previous subset, until the entire dataset is covered. From Fig. 10 it follows that best agreement is found for an average fiber depth of about 30 cm. The least-squares fit method yields solutions that are generally well aligned in phase with the measured data (Fig. 9). However, Fig. 9 also shows that the agreement between the amplitude of the frequency deviations at 30 cm depth and the measured data is poor. The limited agreement may be partially caused by the contribution of fiber dispersion compensation modules, which are located in equipment rooms rather than being buried underground. These modules are located in air-treated environments with stable temperatures, and, although the fiber

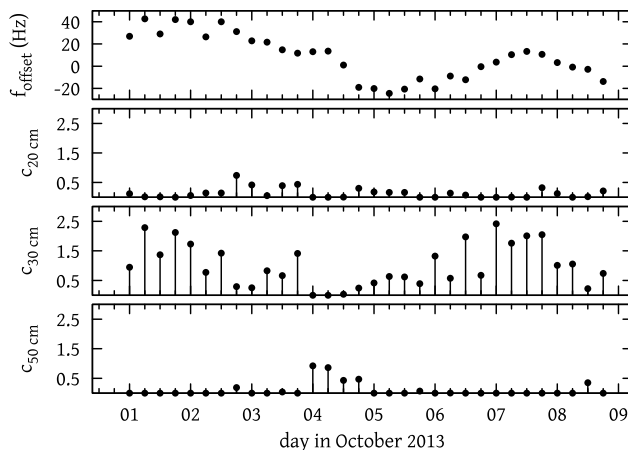


Fig. 10. Fit parameters obtained by least-squares fitting to (partly overlapping) 24 h subsets of round-trip frequency data, with a spacing of 6 h between each subset. Day of year represents the center of the data range. Top, frequency offset for fit. Bottom three panels, values of the  $c_n$  for the most important depths; the  $c_n$  found for the other depths are negligibly small. Averages and standard deviations over this dataset are  $f_{\text{offset}} = 8.1(20.3)$ ,  $c_{20 \text{ cm}} = 0.13(0.17)$ ,  $c_{30 \text{ cm}} = 1.01(0.72)$ , and  $c_{50 \text{ cm}} = 0.10(0.24)$ .

length inside the modules is small compared to the fiber span, thermally induced length changes might have an appreciable effect. This effect will be subject to future study.

In the time series of the link measurement (Fig. 9), the frequency deviations before 3 October and after 6 October appear to follow the predictions based on KNMI data, while between 3 October and 6 October the curves seem to be substantially less correlated. This discrepancy might be linked to the fact that during this period, the fiber-link path received considerably more precipitation on 3 October 2013 than the measurement site at Cabauw [32]. Moreover, solar irradiation differed substantially from day to day between Cabauw and the fiber link in this period [32]. It is conceivable that this led to local soil temperature variations along the fiber link and, thus, to the observed discrepancy. This behavior illustrates the limited power of the temperature model for predicting or estimating instantaneous frequency variations based on soil temperature measurements.

## 2. Soil Temperature Model for Frequency Transfer Stability Estimation

Soil temperature data can be used to predict the long-term stability of fiber links, but it can be burdensome to obtain or construct long historical records. For example, in 1961 soil temperature was measured three times a day [33]. Also, soil temperature is less often measured at meteorological measurement sites than other quantities. In the Netherlands, KNMI has such data available for only four sites. In case of scarce soil temperature data, the sinusoidal soil temperature model [Eq. (5)] can be used to construct an artificial temperature cycle by superposition of a diurnal and an annual temperature cycle, which can be used to estimate the frequency transfer stability of fiber links. Such models can also be used to predict frequency transfer stability for various types of soil.

The amplitude of the diurnal temperature variation itself varies approximately sinusoidally during the year, and is given by

$$A_{T_{d,\text{year}}}(t) = T_{d,\text{year}} + A_{d,\text{year}} \sin\left(\frac{2\pi}{P_{\text{year}}}(t - t_{0,\text{year}})\right), \quad (10)$$

where  $T_{d,\text{year}}$  is the average diurnal temperature variation,  $A_{d,\text{year}}$  is the amplitude of the annual variation of the diurnal amplitude,  $P_{\text{year}}$  is the annual period, and  $t_{0,\text{year}}$  is used to shift the temperature cycle to fit the model to the long-term measurement data of KNMI.

The total annual temperature cycle now becomes

$$T_{\text{annual}}(z, t) = T_0 + T_{\text{day}}(z, t, A_{T_{d,\text{year}}}(t)) + T_{\text{year}}(z, t), \quad (11)$$

where  $T_{\text{day}}$  and  $T_{\text{year}}$  are given by Eq. (5), but now with the amplitude  $A_{T_0}$  of the diurnal variation being a function of time.

Table 1. Parameters of the Soil Temperature Model of Eq. (11) Retrieved by a Least-Squares Fit to Data Obtained from [27] and [33]

	Offset (°C)	Amplitude (°C)	$t_0$ (s)
Annual variation (surface)	10.2	8.8	$9.64 \times 10^6$
Annual day amplitude	2.3	1.4	$7.94 \times 10^6$
$A_{T_{d,\text{year}}}$			
Diurnal variation	0.0	$A_{T_{d,\text{year}}}(t)$	$3.67 \times 10^4$

We obtain a set of model parameters for Eq. (11) by fitting Eq. (5) to the data from Van der Hoeven and Lablans [27] as an estimate of the annual variations, and to the data from Woudenberg [33] to estimate the cycle of diurnal temperature variations. The soil constant was taken as  $C_s = 7.5 \times 10^{-4}$ , which is representative for sand (being in a state between wet and dry), relatively dry loam, and clay [27]. The obtained average, amplitude, and phase values are given in Table 1.

The soil temperatures resulting from the model are plotted in Fig. 11 and compared with the measured KNMI dataset covering the year 2011. The plot compares the data at the surface and at 50 cm depth and shows that the model is indeed in reasonable agreement with direct soil temperature measurements.

Figure 12 compares the frequency stability, computed using Eq. (8), and the soil temperature measurement series of 2011 and 2012 with that obtained from Eq. (8) and the sinusoidal model of Eq. (11). The most prominent feature is the discrepancy for 50 cm depth, likely due to fluctuations in weather conditions on long (days/weeks/months) time scales, which cause a higher instability at time scales between a day and half a year. These fluctuations are clearly visible in Fig. 11. This noise also leads to a smoothing of the strong minima in the

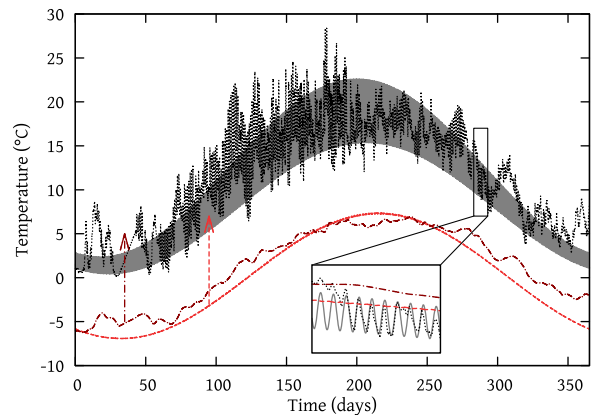


Fig. 11. Annual variation of soil temperature at various depths. Modeled temperature at the surface (solid, appearing as a wide band due to diurnal variations, which are not resolved at the time scale of the plot), and at 50 cm depth (dashed). Measured temperature at the surface (dotted) and at 50 cm depth (dashed-dotted). Temperatures at 50 cm depth are offset by 10 deg centigrade for visibility; arrows indicate true position. The inset shows a 10-day subset of the data to visualize the diurnal variations of the surface temperature.

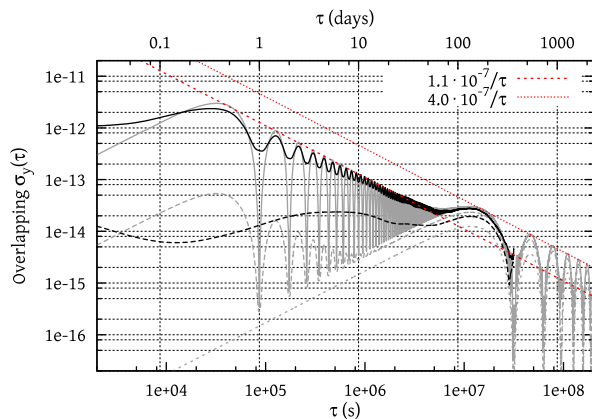


Fig. 12. Frequency stability comparison between soil temperature measurements and the model [Eq. (11)] at several depths: surface measurement (solid), model (solid gray); 50 cm depth measurement (long-dashed), model (long-dashed gray); 200 cm depth model (short-dashed gray). The straight lines indicate the  $1/\tau$  behavior with a maximum instability of  $2.6 \times 10^{-12}$  at half a day for the diurnal variation (dashed) and  $2.5 \times 10^{-14}$  at half a year for the annual variation (dotted) of the sinusoidal model.

frequency instability curves, which are a consequence of the sinusoidal temperature variations of the soil temperature model [Eq. (11)]. The stability at 200 cm depth was calculated from this model and shows that more deeply buried fibers offer a substantial stability improvement at the time scale of days, while the stability at the year scale is much closer to that of fiber buried closer to the surface.

## 5. Conclusions and Outlook

We investigated the passive frequency stability of a  $2 \times 298$  km carrier-grade, unidirectional fiber link between VU University Amsterdam LaserLaB and Van Swinderen Institute, University of Groningen, using a single DWDM channel, and with live optical data traffic present in other DWDM channels. The observed frequency instability of the link lies in the range  $10^{-14}$  to  $10^{-13}$  for averaging times of 10 to  $8 \times 10^5$  s. This result implies that such fiber links are well suited to distribute the frequency of commercial Rb atomic clocks with negligible loss of accuracy. A model for thermo-optical fiber length variation was developed that relates frequency variations to soil temperatures as a function of depth. We employed this model taking actual long-term soil temperature measurements as input, as well as predictions obtained from existing soil temperature models. We combined link frequency measurements with soil temperature measurements at the KNMI Cabauw site to show that the observed link stability corresponds to an average fiber depth of about 30 cm.

Qualitative agreement is found between the soil temperature model and KNMI measurements, while predictions of frequency stability based upon this model agree with actual round-trip frequency measurements to within 1 order of magnitude. Although the predictive power of the soil-temperature model is limited, it does provide insight into the relation

among soil temperature, fiber-optic path length variations, and frequency-transfer stability. Our model thus allows estimating the passive frequency stability of fiber links for averaging times ranging from days to years, and allows estimation of upper bounds on the passive link instability. Such information will be useful for the design of future one-way frequency distribution systems based on underground fiber-optic infrastructure.

The presented results show that soil temperature fluctuations have a large impact on the passive frequency stability of optical carriers over underground fiber links for time scales longer than approximately 1000 s. The results of our study confirm the conclusions of previous work that fiber-optic infrastructure is sufficiently stable for one-way atomic clock frequency distribution over hundreds of kilometers distance, and with  $1 \times 10^{-13}$  relative instability [1,3]. This level of instability compares favorably to the stability of commercial GPS-disciplined Rb clocks. The residual frequency variations are sufficiently small to backup the local oscillator of GPS-referenced clocks with indefinite holdover (provided a non-GPS-referenced master clock is used). This opens up the perspective of a terrestrial “flywheel” oscillator, embedded in the currently installed unidirectional fiber-optic telecommunications network, which can be used to backup GPS-referenced oscillators during periods of GPS outage.

This work was supported by the Netherlands Foundation for Fundamental Research of Matter (FOM) through the program “Broken Mirrors & Drifting Constants.” J.C.J.K. thanks the Dutch Organisation for Scientific Research (NWO) and the Dutch Technology Foundation (STW) for support.

## References

1. P. A. Williams, W. C. Swann, and N. R. Newbury, “High-stability transfer of an optical frequency over long fiber-optical links,” *J. Opt. Soc. Am. B* **25**, 1284–1293 (2008).
2. O. Lopez, A. Amy-Klein, C. Daussy, C. Chardonnet, F. Narbonneau, M. Lours, and G. Santarelli, “86-km optical link with a resolution of  $2 \times 10^{-18}$  for RF frequency transfer,” *Eur. Phys. J. D* **48**, 35–41 (2008).
3. K. Jaldehag, S.-C. Ebenhag, P. O. Hedekvist, and C. Rieck, “Time and frequency transfer using asynchronous fiber-optical networks: progress report,” in *Proceedings of the 41st Annual Precise Time and Time Interval (PTTI) Meeting* (2009), pp. 383–396.
4. G. Grosche, O. Terra, K. Predehl, R. Holzwarth, B. Lipphardt, F. Vogt, U. Sterr, and H. Schnatz, “Optical frequency transfer via 146 km fiber link with  $10^{-19}$  relative accuracy,” *Opt. Lett.* **34**, 2270–2272 (2009).
5. M. Fujieda, M. Kumagai, S. Nagano, A. Yamaguchi, H. Hachisu, and I. Tetsuya, “All-optical link for direct comparison of distant optical clocks,” *Opt. Express* **19**, 16498–16507 (2011).
6. K. Predehl, G. Grosche, S. M. F. Raupach, S. Droste, O. Terra, J. Alnis, T. Legero, T. W. Hänsch, T. Udem, R. Holzwarth, and H. Schnatz, “A 920-kilometer optical fiber link for frequency metrology at the 19th decimal place,” *Science* **336**, 441–444 (2012).
7. O. Lopez, A. Haboucha, B. Chanteau, C. Chardonnet, A. Amy-Klein, and G. Santarelli, “Ultra-stable long distance optical frequency distribution using the internet fiber network,” *Opt. Express* **20**, 23518–23526 (2012).

8. T. Rosenband, D. B. Hume, P. O. Schmidt, C. W. Chou, A. Brusch, L. Lorini, W. H. Oskay, R. E. Drullinger, T. M. Fortier, J. E. Stalnaker, S. A. Diddams, W. C. Swann, N. R. Newbury, W. M. Itano, D. J. Wineland, and J. C. Bergquist, "Frequency ratio of Al<sup>+</sup> and Hg<sup>+</sup> single-ion optical clocks; metrology at the 17th decimal place," *Science* **319**, 1808–1812 (2008).
9. C. W. Chou, D. B. Hume, J. C. J. Koelemeij, D. J. Wineland, and T. Rosenband, "Frequency comparison of two high-accuracy Al<sup>+</sup> optical clocks," *Phys. Rev. Lett.* **104**, 070802 (2010).
10. N. Hinkley, J. A. Sherman, N. B. Phillips, M. Schioppa, N. D. Lemke, K. Beloy, M. Pizzocaro, C. W. Oates, and A. D. Ludlow, "An atomic clock with 10<sup>-18</sup> instability," *Science* **341**, 1215–1218 (2013).
11. B. J. Bloom, T. L. Nicholson, J. R. Williams, S. L. Campbell, M. Bishof, X. Zhang, W. Zhang, S. L. Bromley, and J. Ye, "An optical lattice clock with accuracy and stability at the 10<sup>-18</sup> level," *Nature* **506**, 71–75 (2014).
12. A. Matveev, C. G. Parthey, K. Predehl, J. Alnis, A. Beyer, R. Holzwarth, T. Udem, T. Wilken, N. Kolachevsky, M. Abgrall, D. Rovera, C. Salomon, P. Laurent, G. Grosche, O. Terra, T. Legero, H. Schnatz, S. Weyers, B. Altschul, and T. W. Hänsch, "Precision measurement of the hydrogen 1S–2S frequency via a 920-km fiber link," *Phys. Rev. Lett.* **110**, 230801 (2013).
13. D. W. Hanson, "Fundamentals of two-way time transfer by satellite," in *Proceedings of the 43th Annual Symposium on Frequency Control* (1989), pp. 174–178.
14. V. Zhang, T. E. Parker, J. Achkar, A. Bauch, L. Lorini, D. Matsakis, D. Piester, and D. G. Rovera, "Two-way satellite time and frequency transfer using 1 Mchip/s codes," in *Proceedings of the 41st Annual Precise Time and Time Interval (PTTI) Meeting* (2009), pp. 371–382.
15. D. Piester, A. Bauch, L. Breakiron, D. Matsakis, B. Blanzano, and O. Koudelka, "Time transfer with nanosecond accuracy for the realization of international atomic time," *Metrologia* **45**, 185–198 (2008).
16. D. W. Allan and M. A. Weiss, "Accurate time and frequency transfer during common-view of a GPS satellite," in *Proceedings of the 34th Annual Frequency Control Symposium* (1980), pp. 334–346.
17. V. S. Zhang, T. E. Parker, and M. A. Weiss, "Multi-channel GPS/GLONASS common-view between NIST and USNO," in *Proceedings of the 2000 IEEE / EIA International Frequency Control Symposium and Exhibition* (2000), pp. 598–606.
18. M. A. Lombardi, L. M. Nelson, A. N. Novick, and V. S. Zhang, "Time and frequency measurements using the global positioning system," *Cal. Lab. Int. J. Metrol.* **8**, 26–33 (2001).
19. K. M. Larson and J. Levine, "Carrier-phase time transfer," *IEEE Trans. Ultrason. Ferroelectr. Freq. Control* **46**, 1001–1012 (1999).
20. A. Brown, R. Silva, and E. Powers, "A GPS receiver designed for carrier-phase time transfer," in *Proceedings of ION National Technical Meeting*, Anaheim, California, January, 2000, pp. 32–41.
21. S. Weyers, V. Gerginov, N. Nemitz, R. Li, and K. Gibble, "Distributed cavity phase frequency shifts of the caesium fountain PTB-CSF2," *Metrologia* **49**, 82–87 (2012).
22. T. P. Heavner, E. A. Donley, F. Levi, G. Costanzo, T. E. Parker, J. H. Shirley, N. Ashby, S. Barlow, and S. R. Jefferts, "First accuracy evaluation of NIST-F2," *Metrologia* **51**, 174–182 (2014).
23. L.-S. Ma, P. Jungner, J. Ye, and J. L. Hall, "Delivering the same optical frequency at two places: accurate cancellation of phase noise introduced by an optical fiber or other time-varying path," *Opt. Lett.* **19**, 1777–1779 (1994).
24. E. A. Elias, R. Cichota, H. H. Torriani, and Q. de Jong van Lier, "Analytical soil-temperature model: correction for temporal variation of daily amplitude," *Soil Science Society of America Journal* **68**, 784–788 (2004).
25. K.-C. Lin, C.-J. Lin, and W.-Y. Lee, "Effects of gamma radiation on optical fibre sensors," *IEE Proc. Optoelectron.* **151**, 12–15 (2004).
26. G. Ghosh and H. Yajima, "Pressure-dependent Sellmeier coefficients and material dispersions for silica fiber glass," *J. Lightwave Technol.* **16**, 2002–2005 (1998).
27. P. C. T. van der Hoeven and W. N. Lablans, "Grondtemperaturen," *Wetenschappelijke Rapporten WR-92-05* (Koninklijk Nederlands Meteorologisch Instituut, 1992).
28. R. Emardson, P. O. Hedekvist, M. Nilsson, S.-C. Ebenhag, K. Jaldehag, P. Jarlemark, C. Rieck, J. Johansson, L. R. Pendrill, P. Löthberg, and H. Nilsson, "Time transfer by passive listening over a 10-Gb/s optical fiber," *IEEE Trans. Instrum. Meas.* **57**, 2495–2501 (2008).
29. H. R. Telle, B. Lipphardt, and J. Stenger, "Kerr-lens, mode-locked lasers as transfer oscillators for optical frequency measurements," *Appl. Phys. B* **74**, 1–6 (2002).
30. Made available by Koninklijk Nederlands Meteorologisch Instituut.
31. Koninklijk Nederlands Meteorologisch Instituut (KNMI), "Cesar, Cabauw experimental site for atmospheric research," <http://www.cesar-observatory.nl/>.
32. Koninklijk Nederlands Meteorologisch Instituut (KNMI), "KNMI DataCentrum," <https://data.knmi.nl/>.
33. D. J. P. W. Woudenberg, "Vergelijkende metingen van de grondtemperatuur te De Bilt in 1961," *Tech. Rep.* (KNMI, 1966).